A density functional study of geometry and electronic structures of $[(SiO_4)(M^{III})_2(OH)_2W_{10}O_{32}]^{4-}$, M = Mo, Ru and Rh

David Quiñonero, Keiji Morokuma, Yurii V. Geletii,
Craig L. Hill, Djamaladdin G. Musaev [*]

Cherry L. Emerson Center for Scientific Computation and Department of Chemistry, Emory University, Atlanta, GA 30322, United States

Available online 22 August 2006

Abstract

The effects of redox-active M-atoms (M = Mo, Ru and Rh) of the di-d-transition-metal-substituted γ-Keggin polyoxometalates $[(SiO_4)(M^{III})_2$ $(OH)_2W_{10}O_{32}]^{4-}$, on the geometry and electronic structure of these species were evaluated at the density functional level. It was shown that open isomers (without two bridging OH ligands between the M centers) may coexist with closed isomers (with bridging OHs) only for M = Mo. The ground electronic state of the closed isomer of all the studied species is found to be the singlet $^1A_1$ state in C_{2v} symmetry, but some of the high-spin states are very close in energy. The calculated M–M distance in the ground state increases via M = Mo (2.28 Å) < Ru (2.60 Å) < Rh (3.00 Å). Simultaneously the calculated M–M distances in high-spin states are very similar and are within of 3.13–3.25 Å. The M–$O_{Si}{}^1$ (or M–$O_{Si}{}^2$) bond distances, which vary from 2.00 to 2.17 Å for the ground state of all compounds, elongate upon going to high-spin states. These geometry trends are explained in terms of the frontier orbitals of these species.
© 2006 Elsevier B.V. All rights reserved.

Keywords: Polyoxometalates; γ-Keggin; Redox-active metal

1. Introduction

Polyoxometalates (POMs) are a large class of metal–oxygen cluster anions, the properties of which can be modified by changing their size, shape, charge and chemical composition [1–3]. Most of them possess an extensive and reversible redox chemistry, and some contain multiple unpaired d-electrons that are delocalized to varying degrees in these nanoscale structures. These collective properties of POMs make them useful in catalysis, materials science, magnetochemistry and quantum computing [2,3]. For example, recently, two d-electron-containing redox-active Fe-substituted derivatives of γ-Keggin POMs (M_2-γ-Keggin POM, where M = Fe) were reported to have a remarkable catalytic activity for the oxygenation of different substrates (olefins, alkanes and others) by O_2 or H_2O_2 [4]. However, the mechanisms of these economically and environmentally attractive reactions are still unknown. Knowledge of the geometry and electronic properties of the M_2-γ-Keggin POMs could be invaluable in understanding and controlling this remarkable oxidation

process, as well as designing efficient POM-based materials for emerging technologies.

Toward this goal, we are actively studying the geometry, electronic structure and reactivities of a variety of POMs [5–8]. The present paper is a continuation of our previous theoretical studies and is intended to elucidate the role of the central d-transition metal element M of $[(SiO_4)(M^{III})_2(OH)_2W_{10}O_{32}]^{4-}$, conventionally termed the "heteroatom" in the polyoxometalate literature, on the geometry and electronic structure of these species. We examine the second-row metal derivatives $[(SiO_4)$ $(M^{III})_2(OH)_2W_{10}O_{32}]^{4-}$, M = Mo, Ru and Rh and probe several possible lower-lying electronic states for each M. Clearly the $Mo_2{}^{III}$ compound is not stable with respect to internal electron transfer, i.e. production of $[(SiO_4)(Mo^V)_2(OH)_2(W^{IV})_4(W^{VI})_6$ $O_{32}]^{4-}$ would be spontaneous, but it provides a useful basis of comparison for the $(Ru^{III})_2$ and $(Rh^{III})_2$ derivatives (geometries and electronic structures).

In the literatures, there are basically two classes of Rh-containing polyoxometalates, those involving Rh organometallic units supported on POMs [9–13], and those in which Rh is actually incorporated into the POM units [14–16]. The latter complexes are more appropriately referred to as "Rh polyoxometalates", and these are the complexes of interest in context

---

* Corresponding author. Tel.: +1 404 727 2382; fax: +1 404 727 7412.
E-mail address: dmusaev@emory.edu (D.G. Musaev).
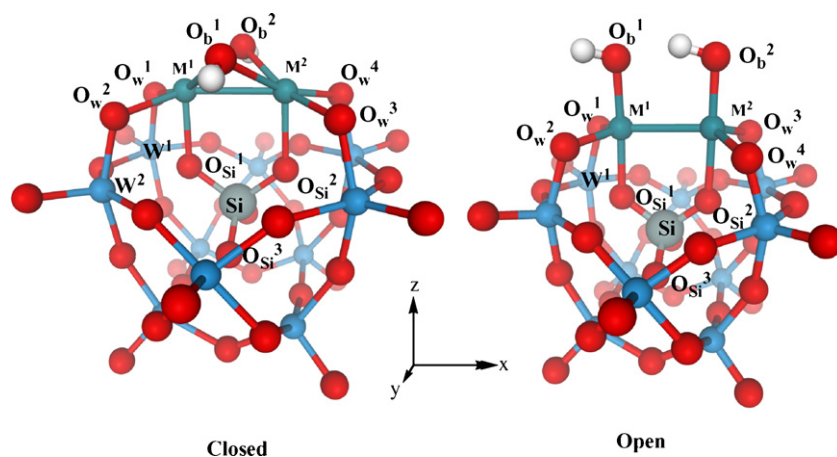
Scheme 1. Schematic presentation of the closed and open isomers of $[(SiO_4)(M^{III})_2(OH)_2W_{10}O_{32}]^{4-}$, with the notations used for the important atoms.

with O_2 activation and selective catalytic oxidation. Rh in these "Rh polyoxometalates" is in the 3+ oxidation state. However, one of the Rh POMs in the former category (Rh unit supported on a polyoxometalate) is a complex reported by Pope and co-workers that contains a Rh(II)$_2$ dimer unit supported on a POM. This is related to our "open" or "out-of-pocket" Rh(III)$_2$ complex [13].

In this paper, we investigate two possible isomers of these species referred to as closed and open (see Scheme 1). The notations of the atoms used in the studied structures are also presented in Scheme 1.

2. Computational methods

In this paper we use the hybrid density functional, B3LYP [17], in conjunction with the lanl2dz basis sets augmented with a set of polarization d function on the central atom X, and associated relativistic effective core potential for all transition metal atoms [18]. We denote the resulting approach as B3LYP/[lanl2dz + d(X)]. Previously we have shown that this approach reasonably describes the electronic and geometric properties of M$_2$-γ-Keggin POMs [5]. Furthermore, in order to validate the use of B3LYP/[lanl2dz + d(X)] approach, we also

calculated geometry and energy gap (ΔE) between the low-spin ($^1A_1$) and high-spin ($^5A_1$) states of $[(SiO_4)(Mo^{III})_2(OH)_2W_{10}O_{32}]^{4-}$: (i) using the non-hybrid BP86 and PW91W91 functionals in conjunction with the [lanl2dz + d(X)] basis set, and (ii) at the B3LYP level with [lanl2dz + d(X and O)] basis set, which in addition to [lanl2dz + d(X)] includes a set of d polarization function for all O atoms.

As seen in Table 1, the inclusion of d polarization functions into the basis set of O atoms only slightly changes the B3LYP/[lanl2dz + d(X)] calculated geometries. Similarly, the use of non-hybrid methods, BP86/[lanl2dz + d(Si)] and PW91PW91/[lanl2dz + d(Si)], does not significantly change the B3LYP/[lanl2dz + d(X)] calculated geometries. However, the use of non-hybrid functionals highly (*ca.* 24 kcal/mol) underestimates the high-spin states. These findings are consistent with our previous conclusions [19], where we also have demonstrated that the B3LYP method provides energetics that is closer to that afforded by the more sophisticated CCSD(T) method. Therefore, below we use only B3LYP/[lanl2dz + d(X)] approach to study the targeted POMs. We optimize the geometries of these species in several of their lower-lying electronic states using the Gaussian 03 program package [20]. The molecular orbitals of the optimized structures were visualized using Molden 3.9 [21].

Table 1

Comparison of the important bond distances (in Å) and the relative energies (ΔE, in kcal/mol) of the $^1A_1$ and $^5A_1$ states of closed isomer of $[(SiO_4)(Mo^{III})_2W_{10}O_{32}]^{4-}$, **1**_closed, calculated at the B3LYP/lanl2dz + d(Si), B3LYP/lanl2dz + d(Si, O), BP86/lanl2dz + d(Si), and PW91PW91 (abbreviated as PW91)/lanl2dz + d(Si) levels, respectively

	$^1A_1$				$^5A_1$			
	B3LYP/ lanl2dz + d(Si)	B3LYP/ lanl2dz + d(Si, O)	BP86/ lanl2dz + d(Si)	PW91/ lanl2dz + d(Si)	B3LYP/ lanl2dz + d(Si)	B3LYP/ lanl2dz + d(Si, O)	BP86/ lanl2dz + d(Si)	PW91/ lanl2dz + d(Si)
Mo–Mo	2.279	2.276	2.304	2.302	2.680	2.672	2.665	2.667
Mo^1–O$_b^1$	2.134	2.134	2.145	2.143	2.132	2.133	2.144	2.140
Mo^1–O$_{Si}^1$	2.179	2.185	2.178	2.175	2.130	2.138	2.140	2.137
Mo^1–O$_W^1$	2.000	1.998	1.996	1.993	2.011	2.010	1.987	1.989
Si–O$_{Si}^1$	1.647	1.645	1.661	1.660	1.654	1.652	1.668	1.667
Si–O$_{Si}^3$	1.647	1.625	1.639	1.637	1.627	1.627	1.640	1.638
ΔE	0.0	0.0	0.0	0.0	0.7	2.7	24.0	23.5

Table 2
Comparison of the important bond distances (in Å) and the relative energies (ΔE, in kcal/mol) of the lower-lying electronic states of $[(SiO_4)(Mo^{III})_2W_{10}O_{32}]^{4-}$, **1**, calculated at the B3LYP/[lanl2dz + d(Si)] level[a]

	1_closed				**1_open**			
	$^1A(^1A_1)$	$^3A(^3B_1)$	$^5A(^5A_1)$	$^7A(^7B_1)$	^1A	^3A	^5A	^7B
Mo–Mo	2.280	2.442	2.677	3.132	2.378	2.697	2.877	3.765
Mo^1–O_b^1	2.134	2.124	2.132	2.142	1.986	2.015	2.025	2.035
Mo^1–O_{Si}^1	2.169	2.115	2.125	2.091	2.278	2.273	2.261	2.201
Mo^1–O_W^1	2.003	2.024	2.015	2.037	1.922	1.907	1.912	1.963
Si–O_{Si}^1	1.647	1.654	1.655	1.662	1.636	1.640	1.643	1.650
Si–O_{Si}^3	1.624	1.622	1.625	1.626	1.633	1.634	1.640	1.643
ΔE	0.0	4.4	0.8	7.9	−1.4	10.5	15.4	31.0

[a] All structures were calculated in C_1 symmetry. However, all final structures have nearly C_{2v} symmetry.

One should note that all singlet state calculations converged to the closed-shell solutions.

Below we discuss the calculated properties of the closed and open isomers of the studied POMs in several of their lower-lying electronic states. For simplicity of our discussions we use the following notation to identify the compounds, isomers and states: n_i_Z, where n stands for the compound [**1**(M = Mo), **2**(M = Ru), and **3**(M = Rh)], i stands for closed or open isomers, and Z stands for the calculated electronic states. Although the optimizations were performed without symmetry constraint, most of the calculations for the closed and open isomers converged to C_{2v} and C_2 symmetry structures, respectively. Therefore, the analysis of molecular orbitals is made mainly at the higher symmetry of these species. The coordinate system used in shown in Scheme 1.

3. Results and discussion

3.1. Geometries, electronic structures and energetics of the $(Mo^{III})_2$-γ-Keggin POM $[(SiO_4)(Mo^{III})_2(OH)_2W_{10}O_{32}]^{4-}$, **1**

The calculated important bond distances of the **1_closed** and **1_open** isomers at their singlet, triplet, quintet and septet states are presented in Table 2. This table also includes the calculated energy differences between the different spin states, as well as between the **1_closed** and **1_open** isomers. Full geometry parameters of these species are presented in Table 1S of the supplementary materials. As seen from Table 2 the energetically lowest electronic states of the **1_closed** isomer are closed-shell singlet and quintet states. The quintet state is only 0.8 kcal/mol higher in energy than the singlet ^1A state. Triplet and septet states are calculated to be 4.4 and 7.9 kcal/mol higher in energy.

The structure of **1_closed_^{1}A** ($^1A_1$ in C_{2v}) has the shortest Mo–Mo bond length (2.280 Å), which is due to the existence of three (one a_1, σ in C_{2v} symmetry, and two π type, one a_1, $\pi_\perp$ and one b_2, $\pi_\parallel$) $Mo^{III}(d^3)$–$Mo^{III}(d^3)$ d–d bonding MOs. The b_2, π_n bonding orbitals involve the d_{xy} and d_{yz} atomic orbitals of the individual Mo atoms, while the a_1, σ and a_1, $\pi_\perp$, bonding orbitals involve the d_{z^2}, $d_{x^2-y^2}$, and d_{xz} orbitals of the Mo center (see Fig. 1), where x-axis defines the M–M bond direction

and the xz plane defines the π reflection plane (Scheme 1). As seen from Fig. 1, the triplet **1_closed_^{3}A** ($^3B_1$ in C_{2v}) state of **1_closed** originates by the promotion of one electron from the HOMO (b_2, $\pi_\parallel$) to the LUMO + 2 (a_2, $\pi_\parallel^*$) antibonding MO. Due to this excitation, the Mo–Mo bond distance elongates to 2.442 Å in **1_closed_^{3}A** from the 2.280 Å in the **1_closed_^{1}A**. As seen from Table 2, other geometry parameters of the system do not change significantly upon the singlet to triplet excitation, except the Mo–O_{Si} bond which contracts from 2.169 Å in **1_closed_^{1}A** to 2.115 Å in **1_closed_^{3}A**. As could be expected, the **1_closed_^{3}A** becomes energetically (by 4.4 kcal/mol) less stable than **1_closed_^{1}A**.

Additional HOMO-1 (a_1, $\pi_\perp$) → LUMO + 3 (b_1, $\pi_\perp^*$) excitation in **1_closed_^{3}A** leads to the quintet state **1_closed_^{5}A** ($^5A_1$ in C_{2v}). As expected, the Mo–Mo bond distance is further elongated to 2.677 Å (0.235 Å with respect to the triplet structure). Changes of the other geometry parameters of **1_closed** upon going from triplet to quintet state structures are insignificant. Interestingly, this second π → π^* excitation is energetically more favorable; the major reason of this, most likely, is the reduction of electron–electron repulsion at the Mo centers. The third excitation, HOMO-2 (a_1, σ) → LUMO + 5 (b_1, σ^*) excitation, leads to the ^{7}A state structure, **1_closed_^{7}A** ($^7B_1$ in C_{2v}) where the Mo–Mo distance is calculated to be much (by 0.455 Å) longer than that in **1_closed_^{5}A**.

The spin density distributions presented in Table 3 confirm the above-discussed electronic configurations. Indeed, in **1_closed_^{3}A** each of the Mo centers have approximately one spin (actual Mulliken spin density: 0.94 e), but it increases to two and three spins (1.88 and 2.78 e) for the quintet and septet states, respectively. The rest of the atoms have negligible unpaired spins, and will not be discussed (they are included in Table 2S of the supplementary materials).

As expected, the Mo–Mo distance is longer for all calculated electronic states of the open isomer of **1**, **1_open**, compared with the corresponding electronic states of the closed isomer **1_closed**. This is result of the lack of two Mo–(OH)–Mo interactions in **1_open**, because OH ligands, bridging between the M centers in the **1_closed**, are in the terminal positions in **1_open**. The terminal location of the OH ligands also provides an explanation for elongation of Mo–O_{Si} bond distances that are trans to
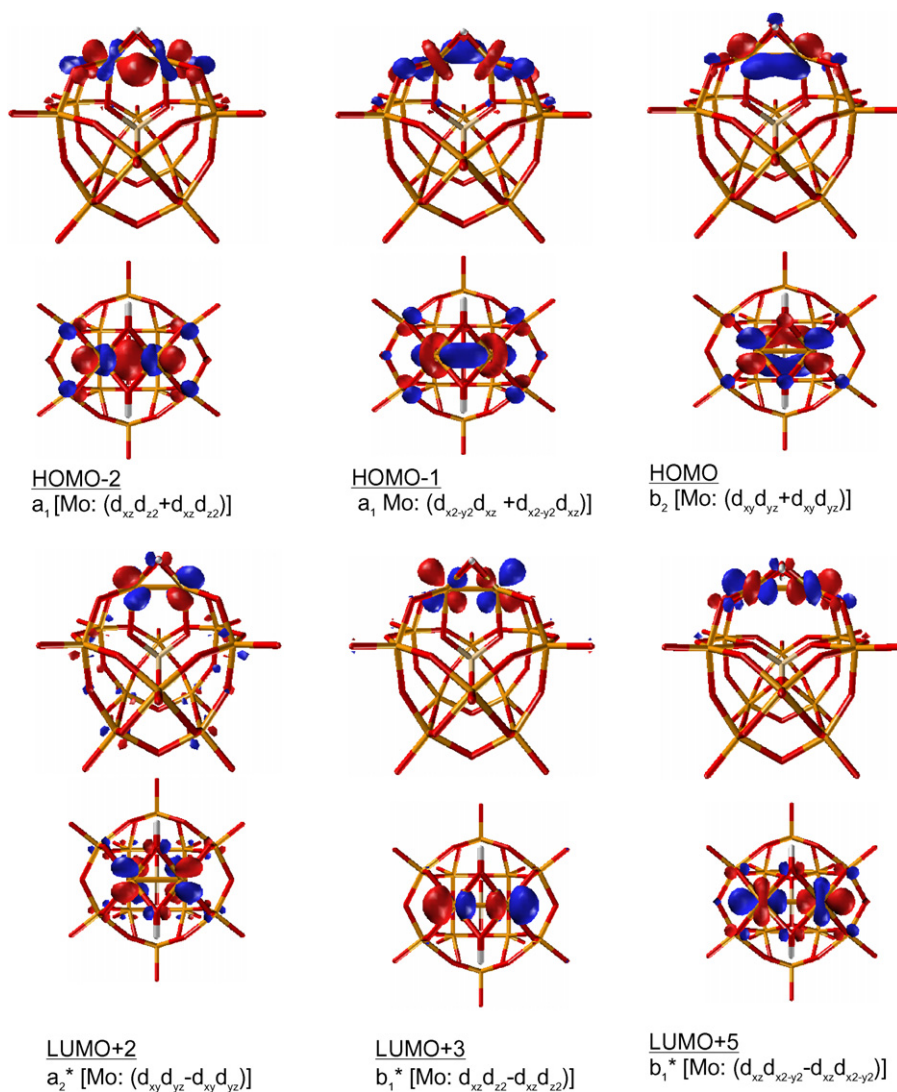
HOMO-2
a_1 [Mo: $(d_{xz}d_{z2}+d_{xz}d_{z2})$]

HOMO-1
a_1 Mo: $(d_{x2-y2}d_{xz} +d_{x2-y2}d_{xz})$]

HOMO
b_2 [Mo: $(d_{xy}d_{yz}+d_{xy}d_{yz})$]

LUMO+2
a_2^* [Mo: $(d_{xy}d_{yz}-d_{xy}d_{yz})$]

LUMO+3
b_1^* [Mo: $d_{xz}d_{z2}-d_{xz}d_{z2})$]

LUMO+5
b_1^* [Mo: $(d_{xz}d_{x2-y2}-d_{xz}d_{x2-y2})$]

Fig. 1. Important HOMO's and LUMO's of $[(SiO_4)(Mo^{III})_2(OH)_2W_{10}O_{32}]^{4-}$, **1**, calculated at the B3LYP/[lanl2dz + d(Si)] level.

the OH ligands. As seen in Table 2, the **1**_open isomer, in general, is energetically less favorable than **1**_closed, except for the singlet state structure. The singlet **1**_open structure is slightly (1.4 kcal/mol) lower in energy than the most stable singlet state of the **1**_closed. As seen in Table 3, each Mo center in **1**_open has

0.98, 1.88 and 2.80 e at its triplet, quintet and septet electronic states. Concluding the present section, calculations show that Mo$_2$-γ-Keggin POM with the singlet ground state could have two different isomers, closed and open, with almost the same energy.

Table 3
The calculated Mulliken atomic spin densities (in e) of the important atoms, as well as $\langle S^2 \rangle$ values of $[(SiO_4)(Mo^{III})_2W_{10}O_{32}]^{4-}$, **1**, in several lower-lying electronic states calculated at the B3LYP/[lanl2dz + d(Si)] level[a]

	1_closed			**1**_open		
	$^3A(^3B_1)$	$^5A(^5A_1)$	$^7A(^7B_1)$	^3A	^5A	^7B
Mo^1	0.94	1.88	2.78	0.98	1.88	2.80
O$_b^1$	0.04	0.00	0.02	0.01	0.02	0.00
O$_{Si}^1$	0.00	0.00	0.00	0.00	0.00	0.00
O$_{Si}^3$	0.00	0.00	0.00	0.00	0.00	0.00
O$_W^1$	0.00	0.01	0.02	−0.02	−0.01	0.01
W^1	0.01	0.03	0.04	0.05	0.06	0.05
$\langle S^2 \rangle$	2.00	6.01	12.02	2.01	6.02	12.02

^a See footnote to Table 2.

Table 4
Comparison of the important bond distances (in Å) and the relative energies (ΔE, in kcal/mol) of the lower-lying electronic states of $[(SiO_4)(Ru^{III})_2(OH)_2W_{10}O_{32}]^{4-}$, **2**, calculated at the B3LYP/[lanl2dz + d(Si)] level[a]

	2_closed						**2_open**			
	$^1A(^1A_1)$	$^3A(^3B_1)$	$^5A(^5B_1)$	$^7A(^7B_1)$	$^9A(^9B_2)$	$^{11}A(^{11}B_1)$	^1A	^3B	^5A	^7B
Ru–Ru	2.598	3.031	3.058	3.066	3.141	3.258	2.607	2.450	2.482	2.862
Ru^1–$O_b{}^1$	2.077	2.097	2.110	2.073	2.085	2.051	1.993	2.017	1.982	1.969
Ru^1–$O_{Si}{}^1$	2.069	2.082	2.090	2.455	2.414	2.415	2.225	2.168	2.111	2.136
Ru^1–$O_W{}^1$	1.995	1.986	1.978	1.999	1.869	1.879	1.884	1.948	2.140	1.859
Si–$O_{Si}{}^1$	1.655	1.661	1.667	1.640	1.657	1.656	1.640	1.637	1.641	1.659
Si–$O_{Si}{}^3$	1.621	1.628	1.637	1.644	1.640	1.636	1.636	1.629	1.626	1.637
ΔE	0.0	2.8	1.9	1.1	32.6	62.1	27.5	28.5	32.5	42.8

[a] All structures were calculated in C_1 symmetry. However, all final structures have nearly C_{2v} symmetry.

3.2. Geometries, electronic structures and energetics of the $(Ru^{III})_2$-γ-Keggin POM $[(SiO_4)(Ru^{III})_2(OH)_2W_{10}O_{32}]^{4-}$, **2**

How will the geometries and electronic structures of M^{III}_2-γ-Keggin POM change upon replacing d^3 Mo(III) centers with d^5 Ru(III) centers? In order to answer this question we study the Ru_2-γ-Keggin POM $[(SiO_4)(Ru^{III})_2(OH)_2W_{10}O_{32}]^{4-}$, **2**. The electronic structures and geometries of the closed isomer were briefly discussed in our previous paper [6]. Here, we include detailed data on this compound for completeness of our discus-

sion on the impact of the nature of redox-active metal centers on the structure and stability of the M_2-γ-Keggin POMs. We calculated the structures of **2** with C_1 and C_{2v} symmetry constraints. The C_1 optimizations of all states with exception of the quintet (^5A) state essentially converge to the structure with *almost* C_{2v} symmetry, the relative energies of which are only 0.1–1.2 kcal/mol lower than their *true* C_{2v} symmetry calculated energies. Their geometry parameters are also almost identical to those obtained for the C_{2v} symmetry constrained structures. Therefore, for simplicity of the discussions below we only
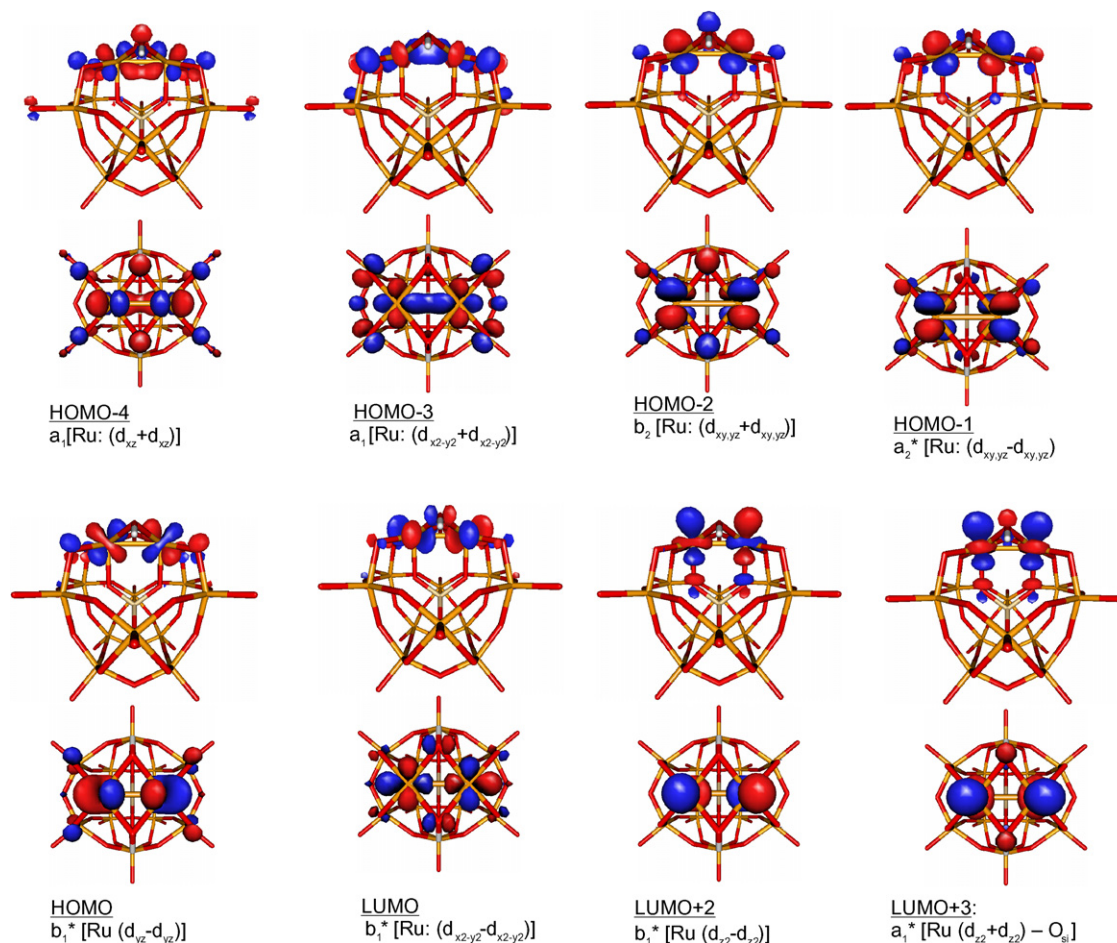

Fig. 2. Important HOMO's and LUMO's of $[(SiO_4)(Ru^{III})_2(OH)_2W_{10}O_{32}]^{4-}$, **2**, calculated at the B3LYP/[lanl2dz + d(Si)] level.

Table 5
The calculated Mulliken atomic spin densities (in e) of the important atoms, as well as $\langle S^2 \rangle$ values of $[(SiO_4)(Ru^{III})_2(OH)_2W_{10}O_{32}]^{4-}$, **2**, in several lower-lying electronic states calculated at the B3LYP/[lanl2dz + d(Si)] level[a]

	2_closed					**2_open**		
	$^3A(^3B_1)$	$^5A(^5B_1)$	$^7A(^7B_1)$	$^9A(^9B_2)$	$^{11}A(^{11}B_1)$	^3B	^5A	^7B
Ru^1	0.82	0.80	2.47	2.74	2.80	0.64	2.25	1.19
Ru^2	0.82	2.48	2.47	2.44	3.79	0.84	0.94	3.52
$O_b{}^1$	0.02	0.07	0.05	0.09	0.16	0.08	0.14	0.09
$O_b{}^2$	0.02	0.01	0.05	0.09	0.16	0.24	0.21	0.33
$O_{Si}{}^1$	−0.02	−0.02	0.09	0.15	0.16	0.00	0.02	0.01
$O_{Si}{}^3$	−0.02	0.00	0.00	0.00	0.00	0.00	0.00	0.00
$O_W{}^1$	0.08	0.08	0.27	0.44	0.43	0.02	0.16	0.20
W^1	0.00	−0.01	0.00	0.08	0.07	0.00	0.00	0.00
$\langle S^2 \rangle$	2.03	6.02	12.02	20.03	30.04	2.04	6.11	12.05

[a] See footnote to Table 4.

present the results obtained under C_{2v} symmetry constraints. In case of the quintet state, the structure with C_1 symmetry is almost 30.2 kcal/mol lower than that with the C_{2v} symmetry. Furthermore, these two structures have very different wavefunctions and geometries (see below for additional discussion). All the calculated geometry parameters are included to supplementary materials (Table 3S).

The calculated major geometry parameters and relative energies of the **2_closed** and **2_open** isomers at their lower-lying electronic states are presented in Table 4. As seen from this table, essentially the calculated singlet, triplet, quintet and septet states of the **2_closed** isomer are very close in energy, which the singlet state being lowest by a slight amount. The ^9A and ^{11}A states lie significantly higher in energy (32.6 and 62.1 kcal/mol, respectively) and will not be discussed in detail.

As seen from Table 4, the $^1A_1$ state structure has the shortest Ru–Ru bond length (2.598 Å). Analysis of the frontiers orbitals of this species shows that this short distance is a result of the existence of two Ru–Ru bonding MOs (see Fig. 2). HOMO-4 with a_1, π symmetry involving $(d_{xz} + d_{xz})$ orbitals of Ru centers, and HOMO-3 with a_1, σ symmetry involving the Ru $(d_{x^2-y^2} + d_{x^2-y^2})$ orbitals. The main difference between the geometries of $^1A_1$ and $^3B_1$ states resides in the Ru–Ru distance, which increases to 3.031 Å (by 0.433 Å) in the triplet state structure. An additional electronic excitation from the nonbonding HOMO-2 $[b_2, (d_{xy,yz} + d_{xy,yz})]$ to the nonbonding LUMO + 2 $[b_1, (d_{z^2} + d_{z^2})]$ yields the $^5A(^5B_2)$ state. Excitation of one electron from the HOMO-3 $[a_1, (d_{x^2-y^2} + d_{x^2-y^2})]$ to LUMO $[b_1, (d_{x^2-y^2} - d_{x^2-y^2})]$ results in the $^7A(^7B_1)$ state of the system. The Ru–Ru distance for ^5A and ^7A states are 3.058 and 3.066 Å, respectively, which are very similar to that for ^3A (3.031 Å). However, there is a substantial difference in the calculated Ru–$O_{Si}{}^1$ (Ru–$O_{Si}{}^2$) bond lengths in these structures. For ^1A, ^3A and ^5A, they are similar (2.069, 2.082 and 2.090 Å, respectively), but for ^7A the calculated Ru–$O_{Si}{}^1$ distances are longer (2.455 Å, respectively).

The spin populations of important atoms are presented in Table 5 (The spin populations of all atoms are presented in Table 4S of the supplementary materials). As seen in this table, the calculated triplet and septet states have almost symmetric wavefunctions with 0.82 e, and 2.47 e unpaired electrons on each

Ru center, respectively. The wavefunctions of the ^9A and ^{11}A states have a slightly asymmetric nature with unpaired electrons on the Ru^1 and Ru^2 centers of 2.74 and 2.44 e for ^9A state, and 2.80 and 3.79 e for ^{11}A state. For the quintet state, the broken-symmetry nature of the obtained wavefunction is very significant; the calculated unpaired electrons on Ru^1 and Ru^2 are 0.80 and 2.48 e, respectively.

The all spin states of the **2_open** isomer of Ru₂-γ-Keggin POM are 28–43 kcal/mol higher in energy than the most stable **2_closed** isomers. The ^9A and ^{11}A states are even higher (not presented in Table 5). These data indicate that it is unlikely the **2_open** isomer of Ru₂-γ-Keggin POM exists, and it will not be discussed in further detail.

3.3. Geometries, electronic structures and energetics of the $(Rh^{III})_2$-γ-Keggin POM $[(SiO_4)(Rh^{III})_2(OH)_2W_{10}O_{32}]^{4-}$, **3**

For this species we have considered the singlet, triplet, quintet, septet and nonet spin states. The C_1 symmetry constraint optimizations for the **3_closed** isomer in the singlet (^1A) and quintet (^5A) states led to structures with C_{2v} symmetry, total energy and atomic spin densities which are almost the same as those obtained in the C_{2v} symmetry constraint calculations. However, optimization of the structure of **3_closed**_^3A under C_1 symmetry constraint converged to a structure with C_s symmetry, which is about 12.9 kcal/mol lower in energy than the C_{2v} optimized structure. Although there has been an energy drop of 10.6 and 4.3 kcal/mol, respectively, on going from C_{2v} to C_1 symmetry constraints for the septet and nonet states, both are still very high in energy compared to the ground singlet state (40.0 and 52.1 kcal/mol, respectively) and will not be discussed below.

The important bond lengths of **3_closed** in several of its lower-lying electronic states, as well as relative energies of these states, are shown in Table 6 (All calculated geometry parameters of **3** are given in Table 5S of the supplementary materials). As seen from this table, the ground state of **3_closed** is the $^1A(^1A_1)$ state, with the $^3A(^3A')$ and $^5A(^5A_1)$ states lying only 2.5 and 4.7 kcal/mol higher in energy. The Rh–Rh bond length of **3_closed**_^1A is calculated to be 3.000 Å, which is the longest

Table 6
Comparison of the important bond distances (in Å) and the relative energies (ΔE, in kcal/mol) of the lower-lying electronic states of $[(SiO_4)(Rh^{III})_2(OH)_2W_{10}O_{32}]^{4-}$, **3**, calculated at the B3LYP/[lanl2dz + d(Si)] level[a]

	3_closed					**3_open**				
	$^1A(^1A_1)$	$^3A(^3A')$	$^5A(^5A_1)$	$^7A(^7B_1)$	$^9A(^9A_1)$	^1A	^3A	^5B	^7B	^9A
Rh–Rh	3.000	2.986	3.000	3.119	3.183	2.681	2.674	2.809	2.895	3.544
$Rh^1-O_b^1$	2.064	2.091	2.097	2.057	2.117	1.973	1.990	2.012	1.954	2.098
$Rh^1-O_{Si}^1$	2.015	2.333	2.383	2.390	2.358	2.120	2.129	2.128	2.092	3.155
$Rh^1-O_W^1$	2.010	1.953	1.953	1.963	1.919	1.940	1.908	1.896	2.001	1.949
$Si-O_{Si}^1$	1.667	1.631	1.643	1.642	1.652	1.647	1.651	1.660	1.662	1.619
$Si-O_{Si}^3$	1.618	1.629	1.643	1.638	1.642	1.629	1.631	1.636	1.634	1.640
ΔE	0.00	2.5	4.7	40.0	52.1	39.0	44.6	52.4	67.9	78.7

[a] All structures were calculated in C_1 symmetry. However, all final structures, except $^3A'$, have nearly C_{2v} symmetry.

M–M bond distance for the singlet states of all POMs addressed in this study. This can be explained by the fact that in the singlet states of compounds **1** and **2**, the $[b_1^*, (d_{x^2-y^2} - d_{x^2-y^2})]$ MO is unoccupied, but in the compound **3** it is doubly occupied.

The promotion of one electron from the antibonding HOMO $[b_1^*, (d_{x^2-y^2} - d_{x^2-y^2})]$ to the antibonding LUMO $[b_1^*, (d_{z^2} - d_{z^2})]$ leads to the $^3A(^3A')$ state for **3_closed**. As it could be

expected, this excitation results in a slight shortening of Rh–Rh distance, but significant elongation of the Rh–O_{Si} distance. For the **3_closed_**^5A, the Rh–Rh distance is calculated to be 3.000 Å, which is very close to those for singlet and triplet states. The calculated Rh–O_{Si} distance in the quintet state is also very close to that in the triplet state. These geometrical features of the quintet state structure are consistent by the fact that the $^5A(^5A_1)$ state
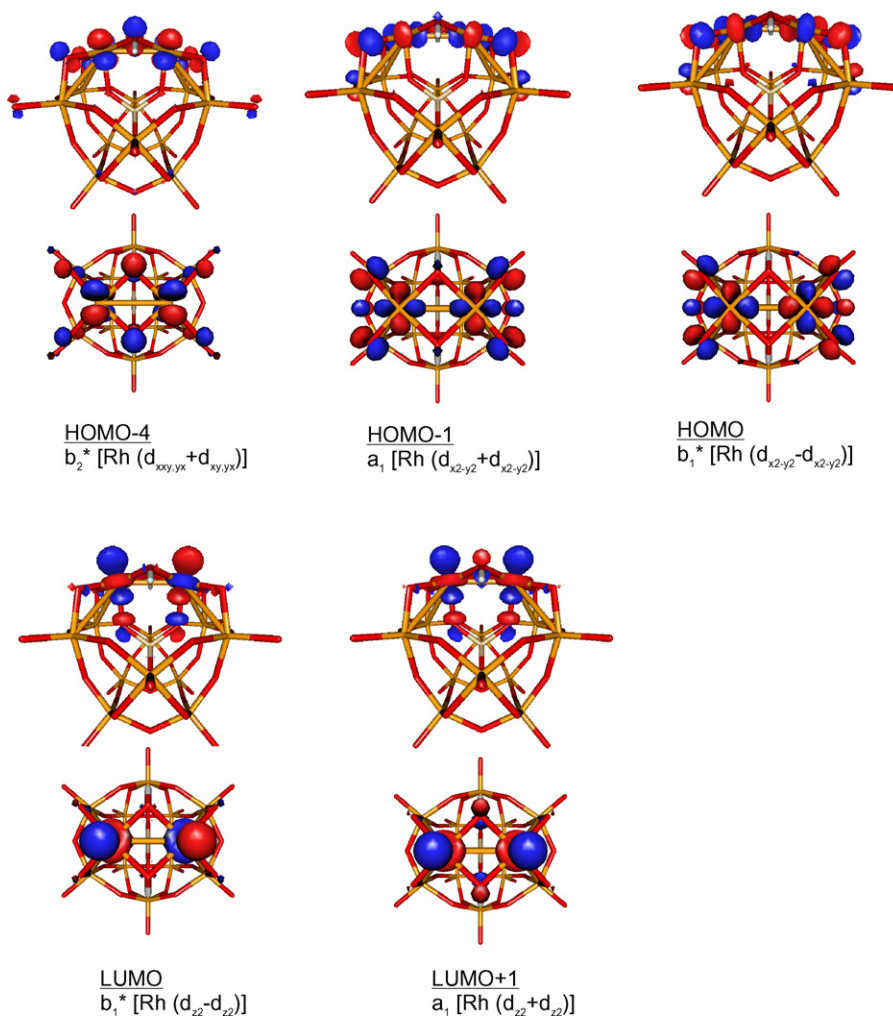

HOMO-4
b_2^* [Rh ($d_{xy,yx}$ + $d_{xy,yx}$)]

HOMO-1
a_1 [Rh ($d_{x^2-y^2}$ + $d_{x^2-y^2}$)]

HOMO
b_1^* [Rh ($d_{x^2-y^2}$ - $d_{x^2-y^2}$)]

LUMO
b_1^* [Rh (d_{z^2} - d_{z^2})]

LUMO+1
a_1 [Rh (d_{z^2} + d_{z^2})]

Fig. 3. Important HOMO's and LUMO's of $[(SiO_4)(Rh^{III})_2(OH)_2W_{10}O_{32}]^{4-}$, **3**, calculated at the B3LYP/[lanl2dz + d(Si)] level.

Table 7
The calculated Mulliken atomic spin densities (in e) of the important atoms, as well as $\langle S^2 \rangle$ values of $[(SiO_4)(Rh^{III})_2(OH)_2W_{10}O_{12}]^{4-}$, **3**, at its several lower-lying electronic states calculated at the B3LYP/[lanl2dz + d(Si)] level[a]

	3_closed				**3_open**			
	$^3A(^3A')$	$^5A(^5A_1)$	$^7A(^7B_1)$	$^9A(^9A_1)$	^3A	^5B	^7B	^9A
Rh^1	1.46	1.45	2.06	2.67	0.27	0.29	1.41	2.60
Rh^2	0.00	1.45	2.09	2.67	1.02	2.38	2.47	2.62
O_b^1	0.00	0.04	0.15	0.31	0.00	0.00	0.16	0.31
O_b^2	0.00	0.04	0.18	0.31	0.19	0.47	0.43	0.31
O_{Si}^1	0.05	0.13	0.14	0.16	0.00	0.00	0.03	0.00
O_{Si}^3	0.00	0.00	0.00	0.01	0.00	0.00	0.00	0.00
O_W^1	0.19	0.20	0.26	0.37	0.11	0.12	0.36	0.26
W^1	−0.01	−0.04	0.00	−0.02	−0.01	−0.01	−0.01	0.00
$\langle S^2 \rangle$	2.03	6.03	12.04	20.03	2.04	6.05	12.04	20.03

[a] See footnote to Table 6.

originated by the promotion of one electron from nonbonding HOMO-1 $[a_1, (d_{x^2-y^2} + d_{x^2-y^2})]$ of Rh to another nonbonding LUMO + 1 $[a_1, (d_{z^2}, d_{z^2})]$ (Fig. 3).

As can be seen from Table 7, the spin densities are essentially located on the Rh atoms. The ^3A state has an asymmetric wavefunction with spin densities of 1.46 and 0.0 e on the Rh^1 and Rh^2 centers, respectively. However, the wavefunction of the quintet, septet and nonet states of **3_closed** are almost symmetric with a 1.45, 2.06 (or 2.09), and 2.67 e on each Rh center, respectively. The remaining spins are distributed on oxygen atoms, and increase with increasing multiplicity of the system (see Table 6S of the supplementary materials for more details).

The open isomers of **3** are energetically highly unstable in the electronic states calculated relative to the singlet ground state of the closed isomer. Therefore, we will not discuss **3_open** in detail; all necessary results are still included in Tables 6 and 7.

4. Conclusions

From the results presented above, one may draw the following conclusions:

1. The open isomer may exist only for $[(SiO_4)(Mo^{III})_2(OH)_2W_{10}O_{32}]^{4-}$, **1**, which is energetically lower or close to the lowest energy state of the closed isomer.
2. The lowest electronic states of $[(SiO_4)(Mo^{III})_2(OH)_2W_{10}O_{32}]^{4-}$, **1** $[(SiO_4)(Ru^{III})_2(OH)_2W_{10}O_{32}]^{4-}$, **2**, and $[(SiO_4)(Rh^{III})_2(OH)_2W_{10}O_{32}]^{4-}$, **3**, are the singlet $^1A_1$ states in C_{2v} symmetry. Some high-spin states of **1_closed** ($^3B_1$ and $^5A_1$ for M = Mo, $^3B_1$, $^5B_1$ and $^7B_1$ for M = Ru, and $^3A'$ and $^5A_1$ for M = Rh) are close in energy to their respective ground low-spin state. As we have shown previously $[(SiO_4)(M^{III})_2(OH)_2W_{10}O_{12}]^{4-}$ for M = Mn and Fe also have a low-spin ground state, while their high-spin states are only a few kcal/mol higher in energy [7].
3. In their low-spin states, the shortest M–M distance in the M_2-γ-Keggin POMs studied here is the di-molybdenum derivative. The M–M distance increases in the order M = Mo (2.280 Å) < Ru (2.598 Å) < Rh (3.000 Å), which correlates with the increase in the number of d-electrons in the system. Simultaneously the calculated M–M distances of the high-

spin states of these species are very similar and range from 3.13 to 3.25 Å, due to nonbonding or very weak antibonding nature of orbitals involved in excitations.
4. Another important geometry parameter of the studied POMs is the M–O_{Si}^1 (or M–O_{Si}^2) bond distance, which ranges from 2.00 to 2.17 Å for the low-spin states of all compounds, but significantly elongates upon going from the low-spin to high-spin states. A similar effect was reported in our previous papers [6,7].

Appendix A. Supplementary data

Supplementary data associated with this article can be found, in the online version, at doi:10.1016/j.molcata.2006.08.034.

References

[1] M.T. Pope, in: A.G. Wedd (Ed.), Comprehensive Coordination Chemistry. II. Transition Metal Groups 3–6, vol. 4, Elsevier Science, New York, 2004, pp. 635–678 (Chapter 4.09).
[2] (a) C.L. Hill, Topical Issue on Polyoxometalates (Guest Ed.), Chem. Rev. 98 (1998) 1;;
(b) C.L. Hill, in: A.G. Wedd (Ed.), Comprehensive Coordination Chemistry II: Transition Metal Groups 3–6, vol. 4, Elsevier Science, New York, 2004, pp. 679–759 (Chapter 4.10);
(c) J.M. Poblet, X. Lopez, C. Bo, Chem. Soc. Rev. 32 (2003) 297–308.
[3] M.T. Pope, A. Müller (Eds.), Polyoxometalate Chemistry: From Topology via Self-assembly to Applications, Kluwer, Dordrecht, The Netherlands, 2001.
[4] (a) Y. Nishiyama, Y. Nakagawa, N. Mizuno, Angew. Chem. Int. Ed. 40 (2001) 3639;
(b) I.V. Kozhevnikov, Catalysis by Polyoxometalates, Wiley & Sons, Chichester, England, 2002.
[5] D.G. Musaev, K. Morokuma, Y.V. Geletii, C.L. Hill, Inorg. Chem. 43 (2004) 7702.

[6] D. Quinonero, Y. Wang, K. Morokuma, L.A. Khavrutskii, B. Botar, Y.V. Geletii, C.L. Hill, D.G. Musaev, J. Phys. Chem. B 110 (2006) 170–173.

[7] Y. Wang, G. Zheng, K. Morokuma, Y.V. Geletii, C. Hill, D.G. Musaev, J. Phys. Chem. B 110 (2006) 5230–5237.

[8] R. Prabhakar, K. Morokuma, C.L. Hill, D.G. Musaev, Inirg. Chem. 45 (2006) 5703–5709.

[9] C.J. Besecker, V.W. Day, W.G. Klemperer, M.R. Thompson, J. Am. Chem. Soc. 106 (1984) 4125–4136.

[10] M.N. Vargaftik, Y.T. Struchkov, A.I. Yanovsky, P.M. Maitlis, Mendeleev Commun. (1993) 247–249.

[11] M. Pohl, Y. Lin, T.J.R. Weakley, K. Nomiya, M. Kaneko, H. Weiner, R.G. Finke, Inorg. Chem. 34 (1995) 767–777.

[12] T. Nagata, B.M. Pohl, H. Weiner, R.G. Finke, A.R. Siedle, R.A. Newmark, W.B. Gleason, R.P. Skarjune, K.O. Hodgson, A.L. Roe, V.W. Day, Solid State Ionics 26 (1988) 109–117.

[13] X. Wei, M.H. Dickman, M.T. Pope, Inorg. Chem. 36 (1997) 130–131.

[14] R. Neumann, A.M. Khenkin, J. Mol. Catal. A: Chem. 114 (1996) 169–180.

[15] F. Zonnevijlle, C.M. Tourné, G.F. Tourné, Inorg. Chem. 21 (1982) 2751–2757.

[16] Y. Matsumoto, M. Asami, M. Hashimoto, M. Misono, J. Mol. Catal. A: Chem. 114 (1996) 161–168.

[17] (a) A.D. Becke, Phys. Rev. A 38 (1988) 3098–3107;
(b) A.D. Becke, J. Chem. Soc. 98 (1993) 1372–1380;
(c) C. Lee, W. Yang, R.G. Parr, Phys. Rev. B 37 (1988) 785–789.

[18] (a) P.J. Hay, W.R. Wadt, J. Chem. Phys. 82 (1985) 299–310;
(b) P.J. Hay, W.R. Wadt, J. Chem. Phys. 82 (1985) 270–283;
(c) W.R. Wadt, P.J. Hay, J. Chem. Phys. 82 (1985) 284–298.

[19] I.V. Khavrutskii, D.G. Musaev, K. Morokuma, Inorg. Chem. 42 (2003) 2606.

[20] M.J.T. Frisch, et al., Gaussian_2003, Gaussian Inc., Pittsburgh, PA, 2003.

[21] G. Schaftenaar, J.H. Noordik, J. Comput. Aid. Mol. Design 14 (2000) 123.